# Supporting Information

**Deep Neurotherapeutic Strategy for Ischemic Stroke via Focused Ultrasound-Enhanced Delivery of Curcumin-Loaded Antioxidant Nanoliposomes**

*Ting-Yi Su,†[a] Ming-Yang Chang,†[a] Guan-Tsz Huang,[b] Wen-Tse Huang,[a] Yu-Ling Lin,[c] ChaoChin Su,[b,*] Ming-Hsien Chan,[d,*] Ming-Yen Hsiao,[c,*] and Ru-Shi Liu[a,*]*

[a] Department of Chemistry, National Taiwan University, Taipei 106, Taiwan

[b] Institute of Organic & Polymeric Materials, National Taipei University of Technology, Taipei 106, Taiwan

[c] Department of Physical Medicine and Rehabilitation, National Taiwan University Hospital, College of Medicine, National Taiwan University, Taipei 100, Taiwan

[d] Department of Biomedical Imaging and Radiological Sciences, National Yang Ming Chiao Tung University, Taipei 112, Taiwan

## Supplementary Figures

**Supplementary Figure S14 |** Raw data of the Western blot in Figure 7b

**Supplementary Figure S15 |** IHC staining of brain sections using NeuN

**Supplementary Figure S16 |** H&E staining of ischemic and contralateral brain regions

**Supplementary figures**

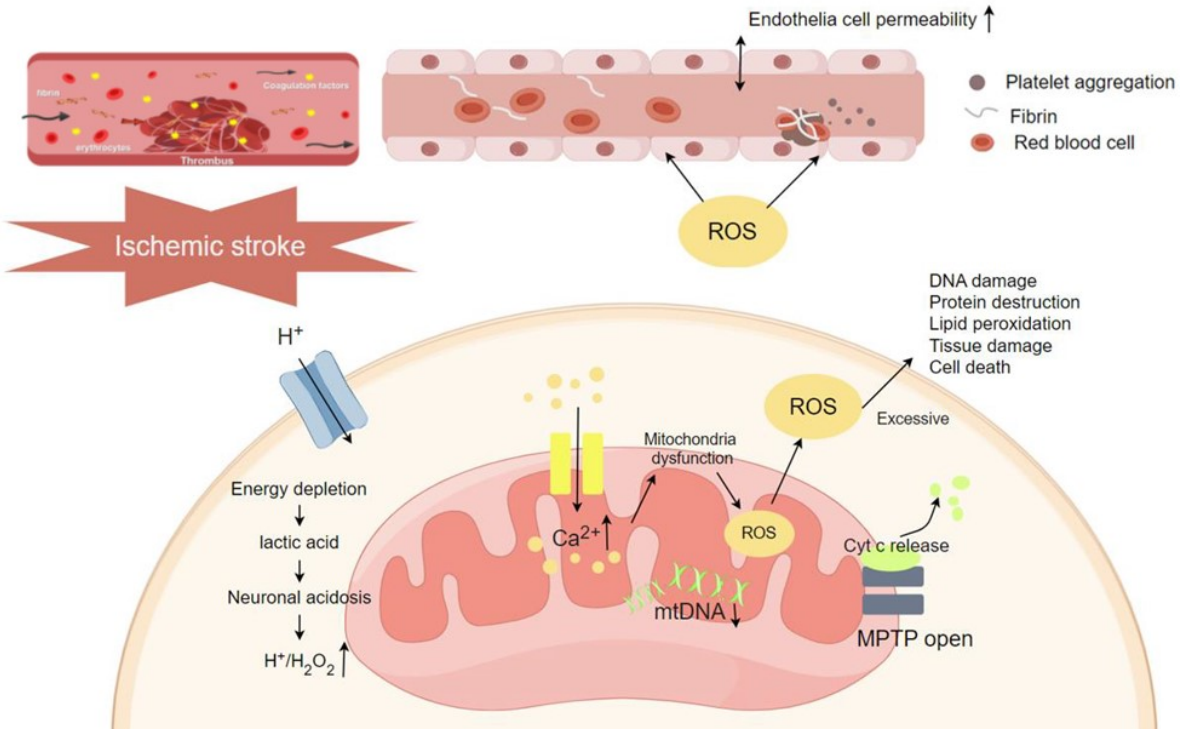


**Figure S1**. A schematic illustration showing the process of thrombus formation and the underlying oxidative stress mechanism involved in ischemic stroke. The diagram highlights how a blood clot can obstruct cerebral blood flow, leading to oxygen and nutrient deprivation, which subsequently triggers oxidative stress and neuronal damage in the affected brain region.

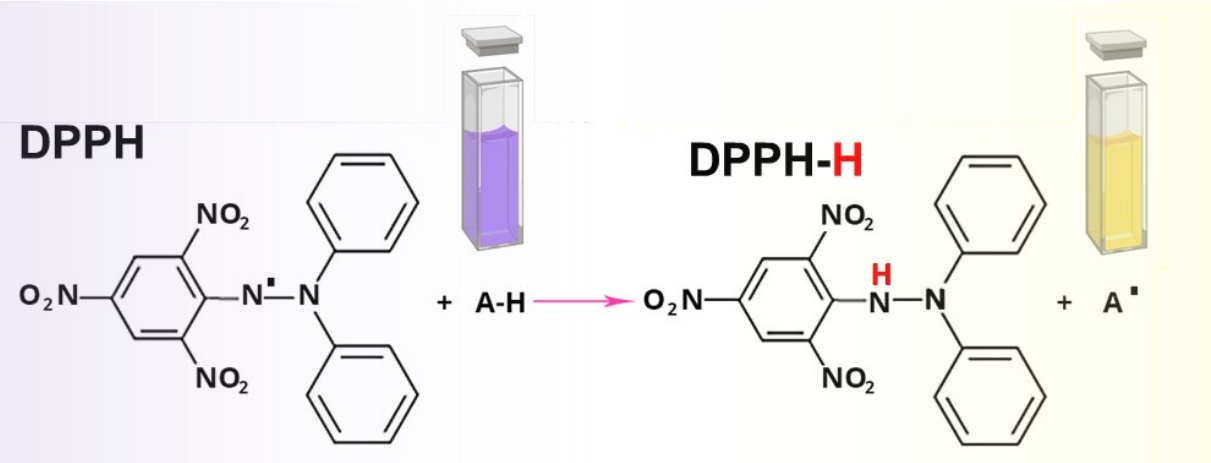


**Figure S2.** Hydrogen atom transfer (HAT) mechanism of DPPH radical scavenging. The antioxidant (AH) donates a hydrogen atom to the DPPH radical (DPPH•), resulting in the formation of the reduced form (DPPH-H) and a corresponding antioxidant radical (A•).

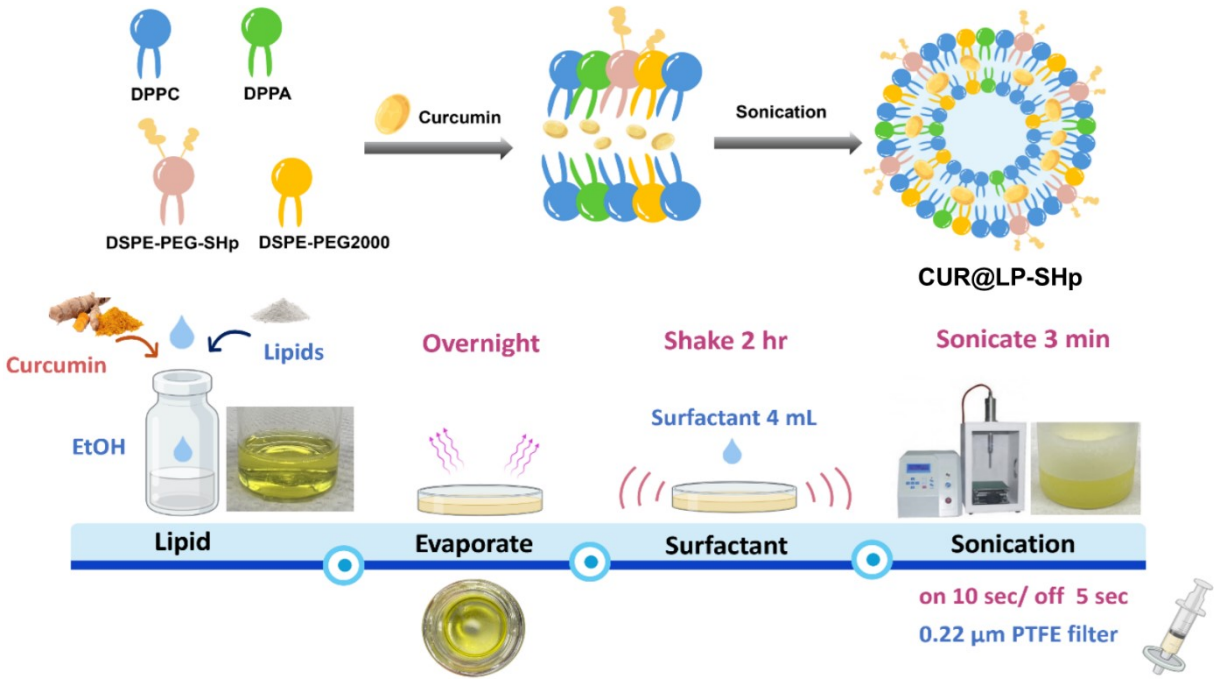


**Figure S3**. A schematic diagram illustrating the synthesis process of ischemic stroke-targeted curcumin-loaded liposomes (CUR@LP-SHp). The formulation, CUR@LP-SHp, is designed to enhance the targeted delivery of Cur to ischemic brain regions, aiming to improve therapeutic efficacy through its antioxidant and neuroprotective properties.

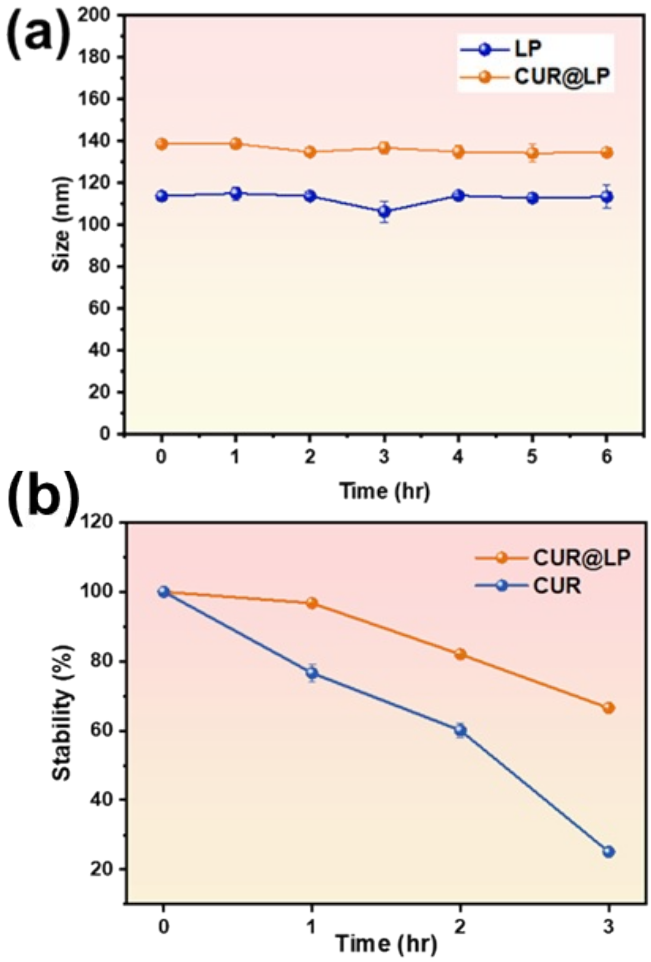


**Figure S4**. The thermal stability of liposomal formulations and free CUR under physiological temperatures. (a) Stability analysis of LP and CUR@LP at 37°C (n = 3). (b) Stability analysis of the antioxidant drug CUR@LP compared to free Cur at 37°C (n = 3).

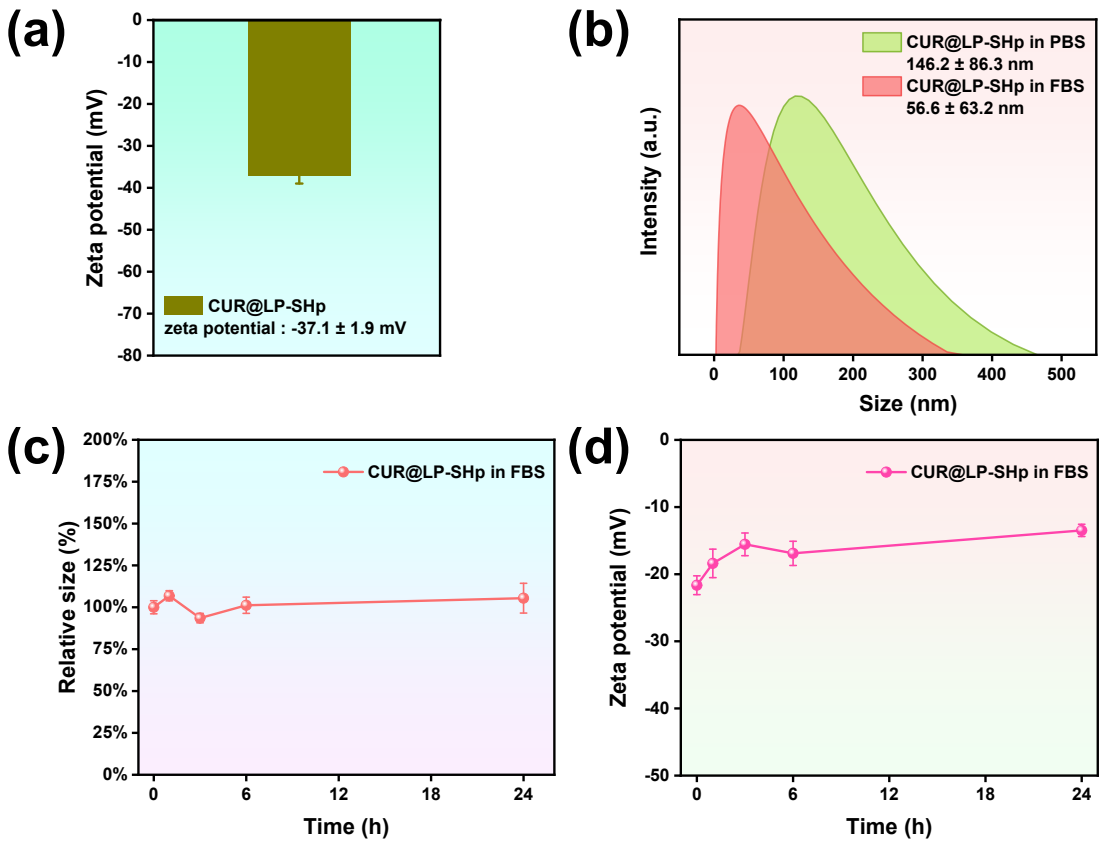


**Figure S5**. The characteristics of modified liposomes. (a) Zeta potential of CUR@LP-SHp (n = 3). (b) Size distribution of CUR@LP-SHp in PBS and in an equal volume of FBS. Serum stability of CUR@LP-SHp in (c) size distribution (n = 3) and (d) zeta potential (n = 3).

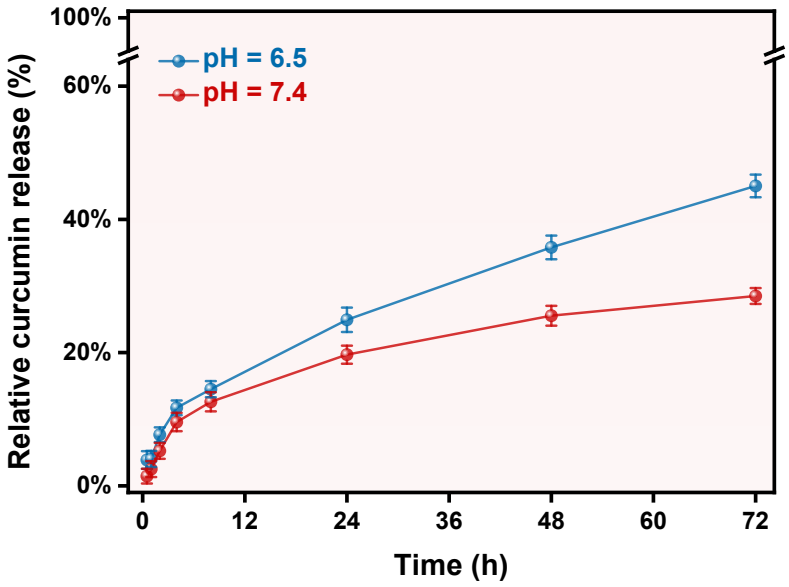


**Figure S6**. *In vitro* drug release analysis of the sample under simulated physiological (pH = 7.4) and ischemic (pH = 6.5) environments over 72 hours (n = 3).

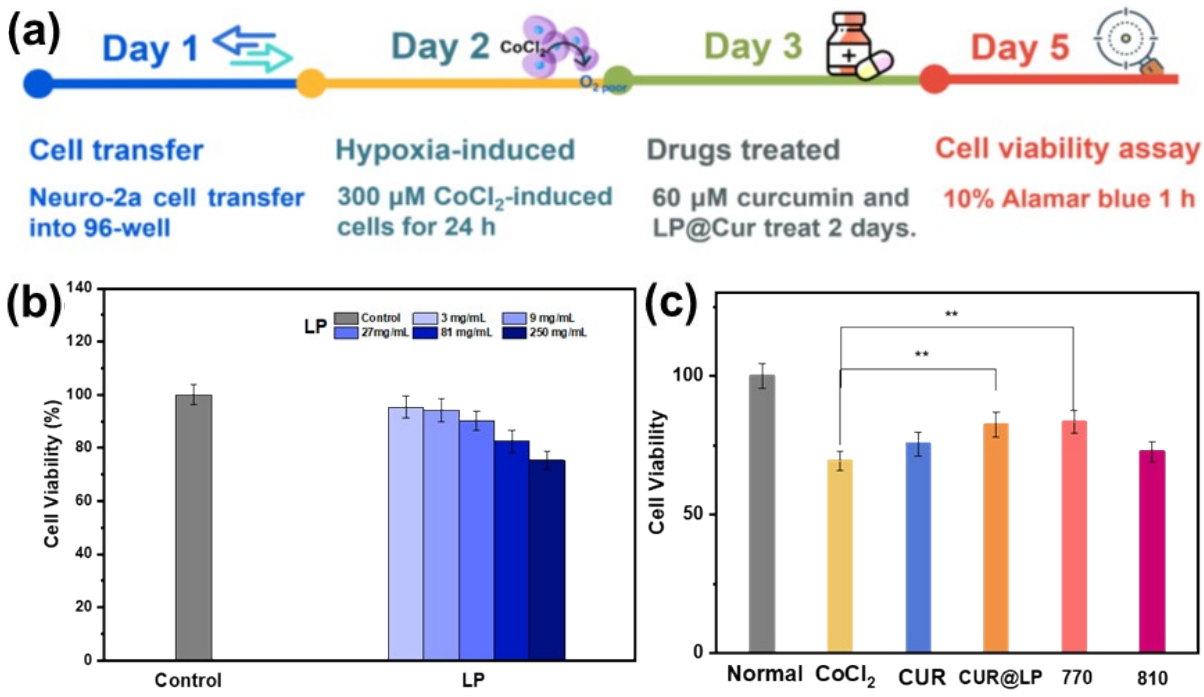


**Figure S7**. Cell viability analysis of normal Neuro-2a cells and $CoCl_2$-induced hypoxic cells treated with Cur and CUR@LP, respectively. (a) Timeline diagram of the treatment process of $CoCl_2$-induced hypoxic cells with antioxidant drugs. (b) Biocompatibility analysis of nanoliposomes with normal Neuro-2a cells (n = 8). (c) Cell viability of the control group (normal cells), $CoCl_2$ group (hypoxic cells), and hypoxic cells treated with 60 μM Cur and CUR@LP (n = 8). (The significance is marked as $^{**}p<0.01$ compared to the control group.)

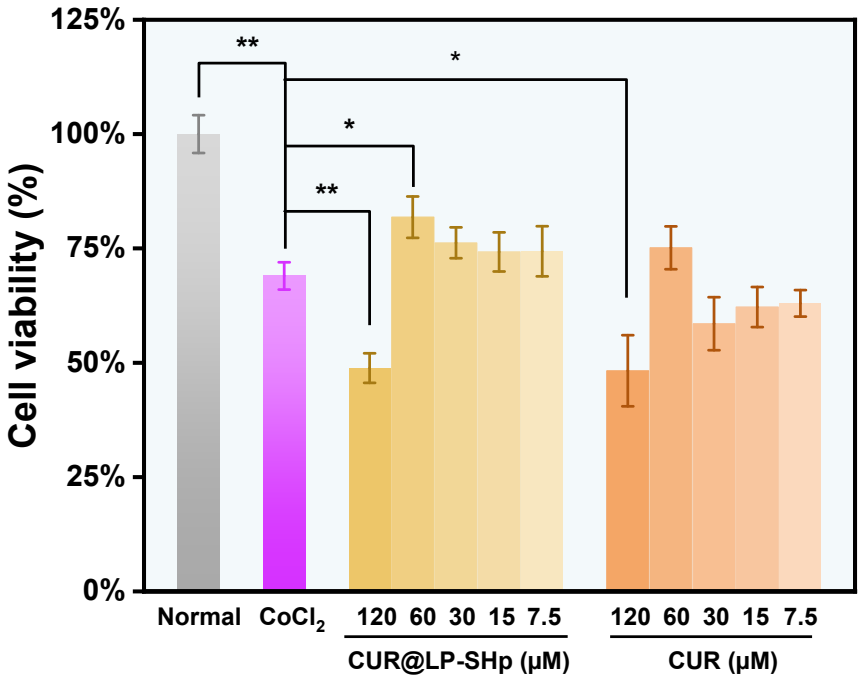


**Figure S8**. Cell viability of normal and $CoCl_2$-induced hypoxic Neuro-2a cells treated with various concentrations of CUR@LP-SHp and free CUR (n = 8). (The significance is marked as *$p$<0.05 and **$p$<0.01 compared to the control group.)

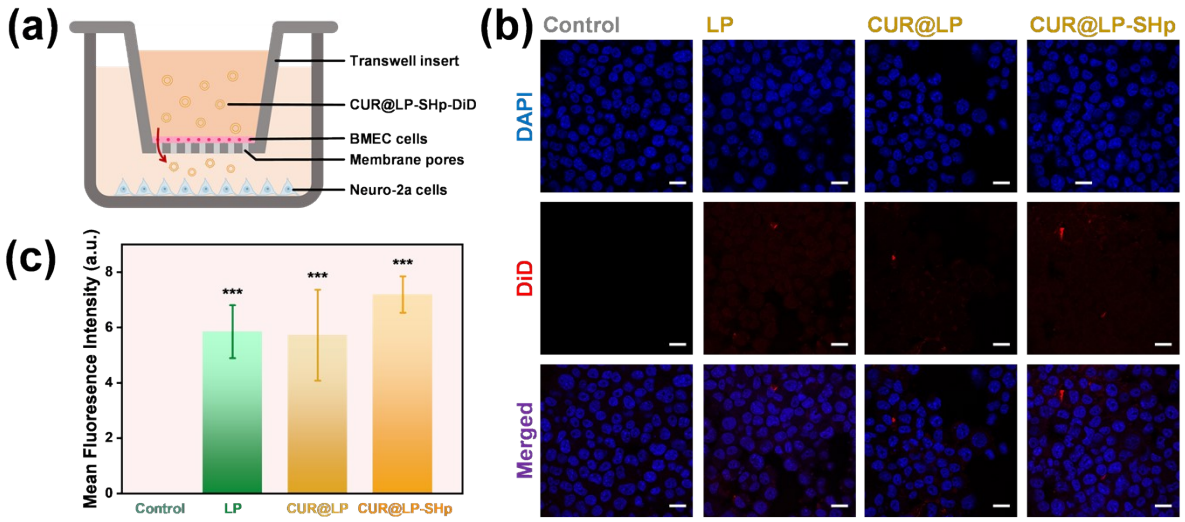


**Figure S9**. (a) The scheme of the blood-brain barrier-mimicked transwell system. (b) Confocal microscopy images and (c) quantitative results of DiD-labeled liposome across the BBB penetration (n = 6). (The significance is marked as ***$p$<0.001 compared to the control group. Scale bar = 20 μm)

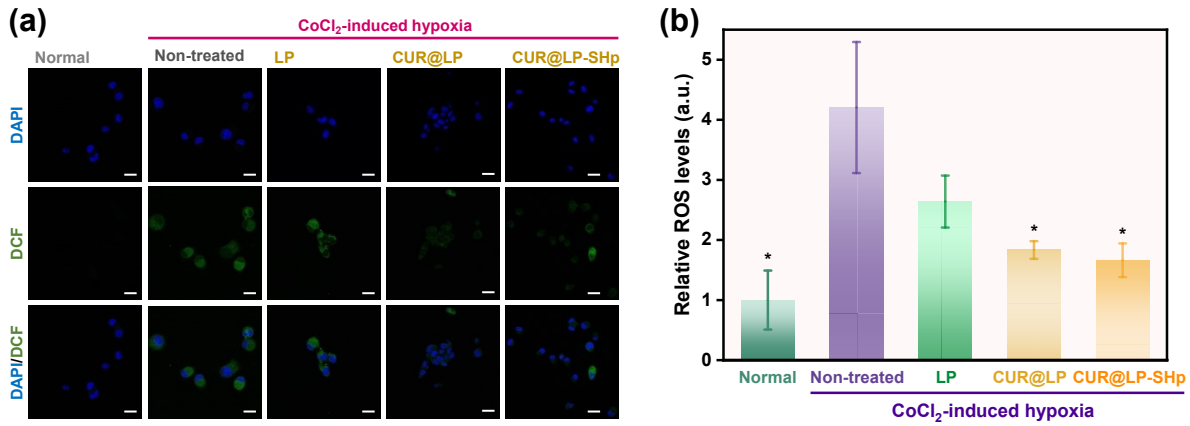


**Figure S10**. (a) Confocal microscopy images of DCF staining for ROS detection to investigate the antioxidant effects of LP, CUR@LP, and CUR@LP-SHp in $CoCl_2$-induced hypoxic Neuro-2a cells and (b) quantitative results of fluorescence intensity in the images (n = 6). (The significance is marked as *$p$<0.05 compared to the control group. Scale bar = 20 μm)

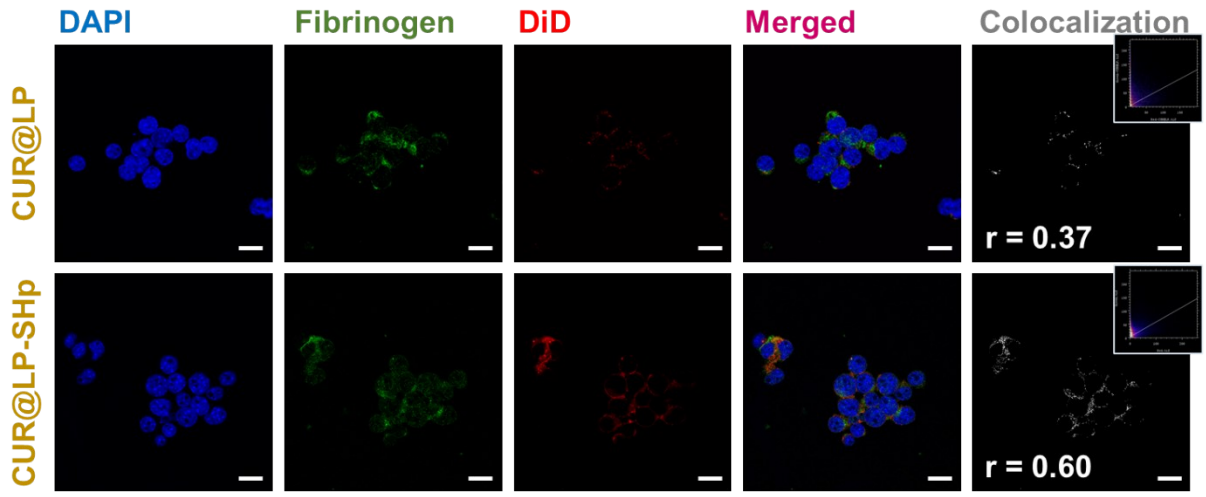


**Figure S11**. Confocal colocalization of DiD-labeled CUR@LP and CUR@LP-SHp with fibrinogen. (Scale bar = 20 μm)

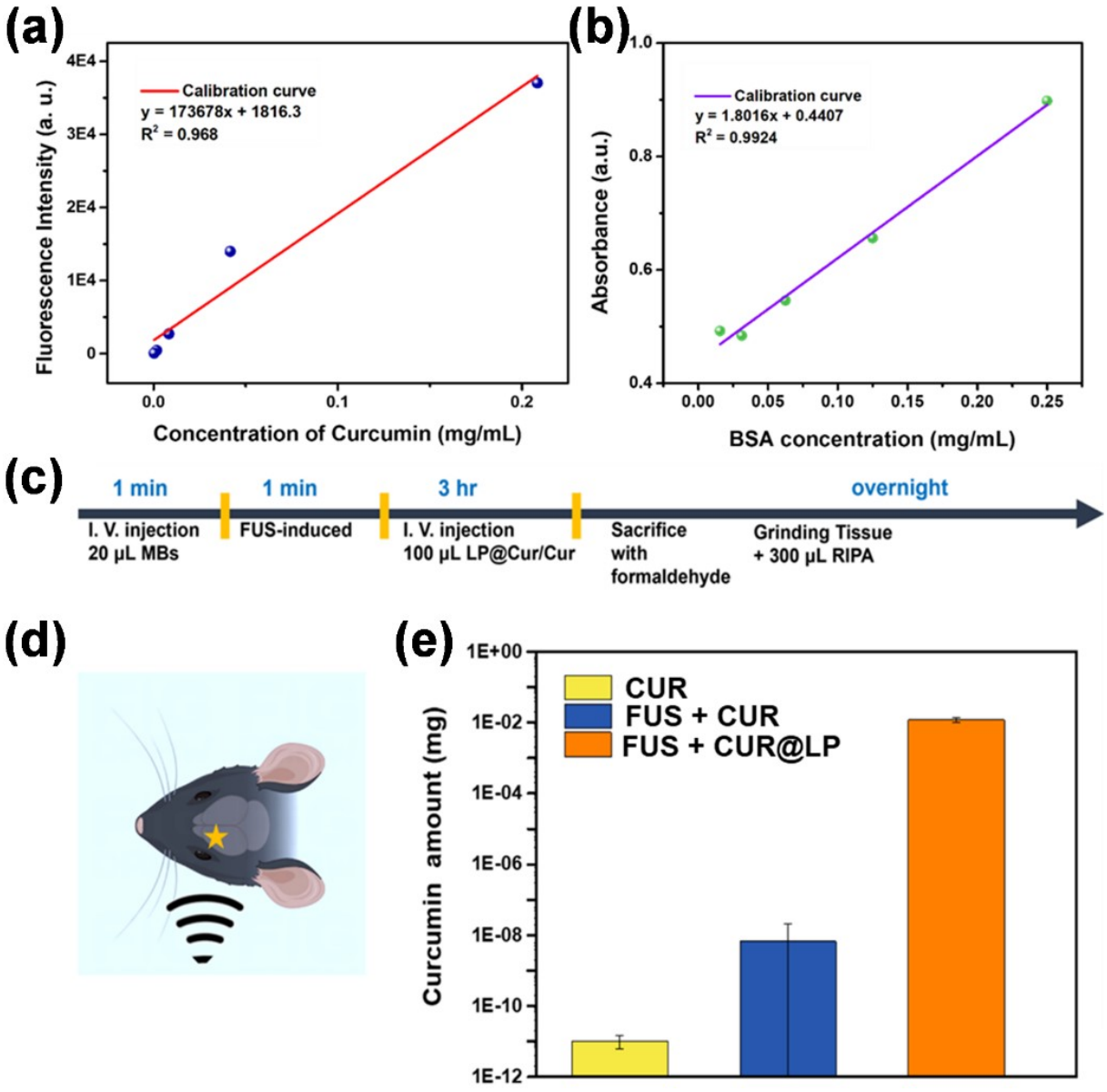


**Figure S12.** (a) CUR fluorescence intensity-concentration calibration curve. (b) BSA absorption-concentration calibration curve. (c) Experimental protocol flow chart and (d) scheme of drug accumulation. (e) Chart of drug accumulation (n = 3).

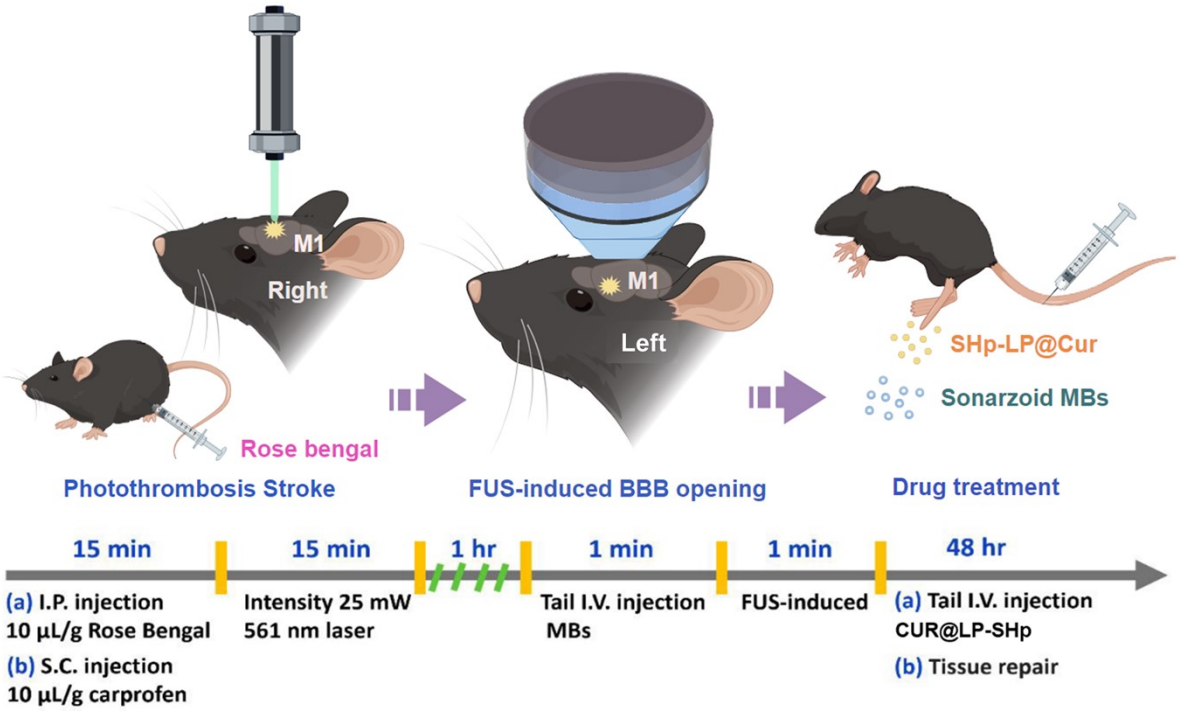


**Figure S13**. A schematic diagram illustrating the treatment process of photothrombotic ischemic stroke using focused ultrasound combined with liposomal drug delivery. This approach leverages the ability of focused ultrasound to temporarily increase blood-brain barrier permeability, enabling the targeted delivery of CUR@LP-SHp to the ischemic brain tissue, thereby enhancing treatment effectiveness.

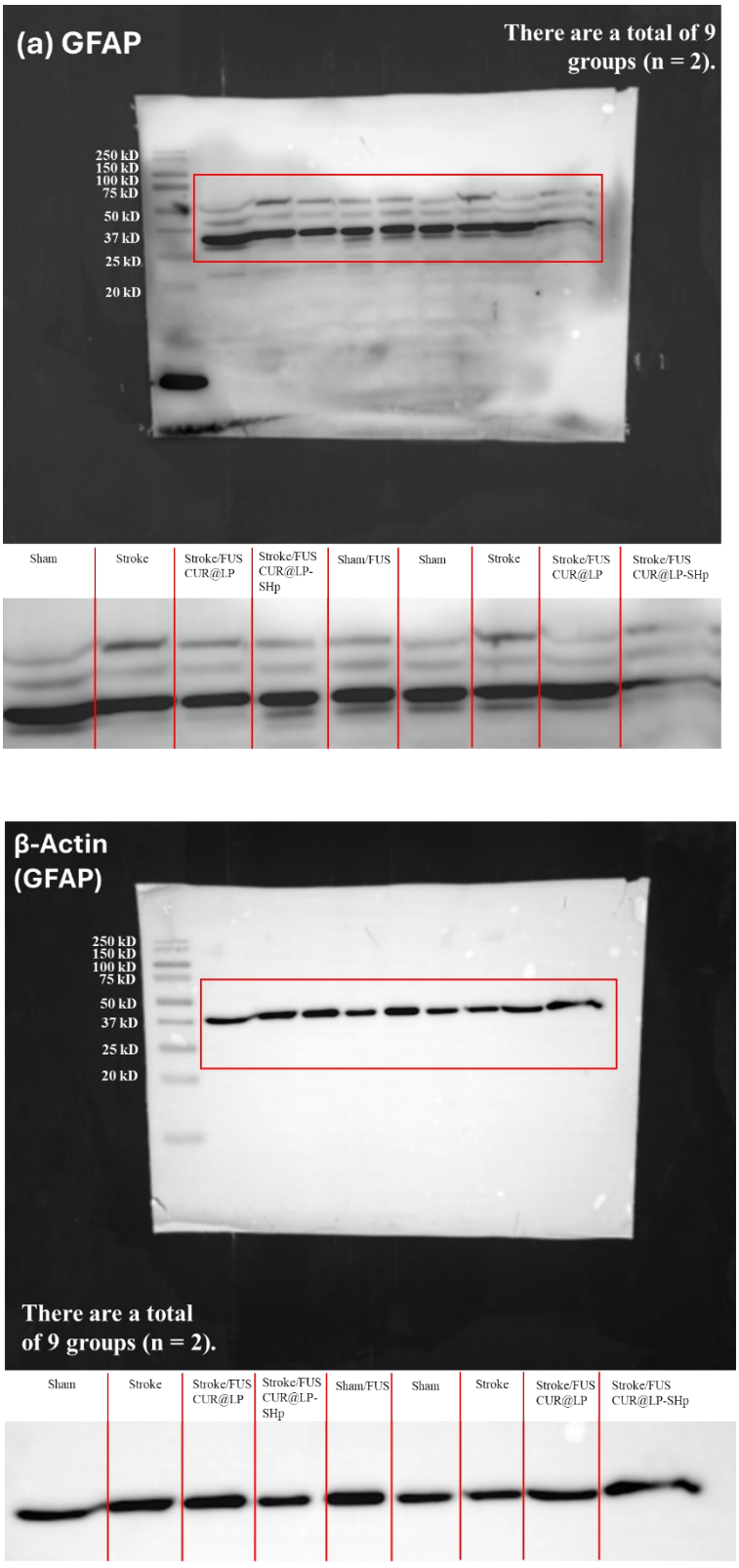


**Figure S14**. Raw data of the Western blot in Figure 7. Original uncropped Western blot images for GFAP and β-actin are shown in Figure 7b. Each image displays molecular weight markers and lane labels for sample identification (n = 2).

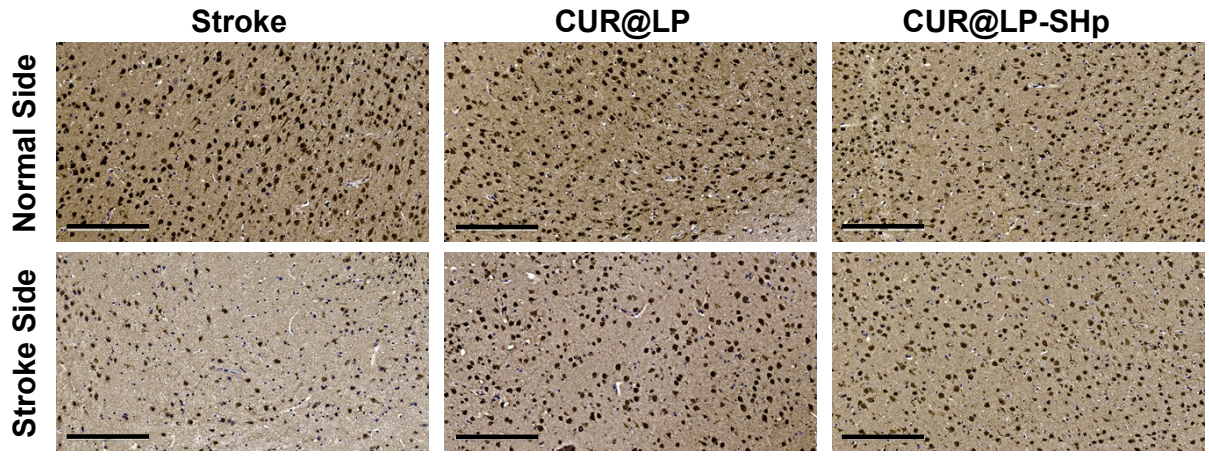


**Figure S15**. IHC staining of brain sections using NeuN as a neuronal marker. (Scale bar = 200 μm)

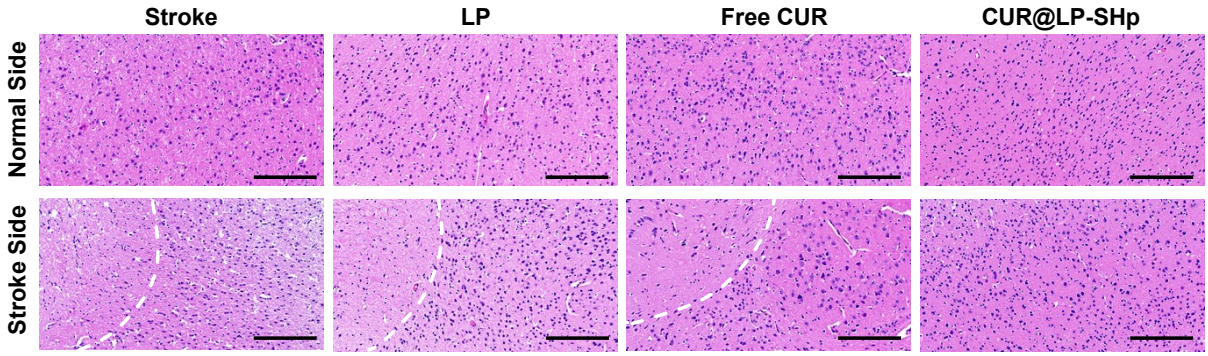


**Figure S16**. H&E staining of ischemic and contralateral brain regions in stroke mice after different treatments. White dashed lines indicate the boundary between ischemic regions and surrounding healthy tissue. (Scale bar = 200 μm)